PPT1 Deficiency-Induced GABAAR Hyperpalmitoylation Impairs Synaptic Transmission and Memory Formation

Jia Tong
Xinxiang Medical University
Jingjing Gao
Xinxiang Medical University
Bingyan Feng
Xinxiang Medical University
Xing Zhao
Xinxiang Medical University
Junmei Li
Xinxiang Medical University
Yawei Qi
Xinxiang Medical University
Qiuyu Zhang
Xinxiang Medical University
Chengbiao Lu
Xinxiang Medical University
Shiyong Peng (171012@xxmu.edu.cn)
Xinxiang Medical University https://orcid.org/0000-0003-0697-3674

Research Article

Keywords: GABAAR, depalmitoylation, palmitoyl protein thioesterase 1, inhibitory postsynaptic current, γ oscillation, infantile neuronal ceroid lipofuscinosis.

Posted Date: March 24th, 2022

DOI: https://doi.org/10.21203/rs.3.rs-860958/v2

Abstract

Palmitoylation is a reversible and dynamic process involving addition of palmitic acid to cysteine residues of proteins. Studies have indicated that a variety of neuronal receptors, including glutamate receptors such as AMPAR, NMDAR, and $GABA_AR$, are palmitoylated, which contributes to the dynamic modulation of synaptic strength in response to neuronal activity. However, little is known about the depalmitoylation of these receptors. In this study, we adopted PPT1-deficient mice, an animal model that closely mimics human disease of infantile neuronal ceroid lipofuscinosis (INCLs), by knocking in a *CLN1* c.451C > T nonsense mutation. We identified for the first time that the $GABA_AR$α1 subunit rather than AMPAR is the substrate of PPT1. In PPT1-deficient mice, we found the excessive palmitoylation and extended membrane location of $GABA_AR$. Miniature inhibitory postsynaptic current (mIPSC) recorded from CA1 pyramidal neurons of PPT1-KI mice was also enhanced without disturbance of excitatory neuronal transmission. Spatial learning and memory deficits with enhancement of γ oscillation while attenuation of phase coupling was shown in the mice at as early as 2-month-old. Application of *N-tert*-butylhydroxylamine hydrochloride, a thioesterase mimetic, attenuated PPT1 mutation-induced $GABA_AR$ hyperpalmitoylation and its membrane accumulation with improved neuronal transmission and memory functions in the mice. These data provide new insights into the mechanisms of neuronal disorder caused by depalmitoylation deficiency and offer a clue for further intervention for INCLs and other neurodegenerative diseases.

Introduction

Palmitoylation is a post-translational modification in which a long-chain, 16-carbon fatty acid (palmitate) is attached to the thiol groups of cysteine residues in substrate proteins [1]. Palmitoylation regulates the distribution of substrate proteins between the plasma membrane and the cytoplasm and the coupling of signaling molecules to cell surface receptors or intracellular effectors [2–8]. Protein palmitoylation is executed by palmitoyl acyltransferases, enzymes containing a zinc finger domain with a conserved DHHC (Asp-His-His-Cys) motif (zDHHCs) [9, 10], whereas depalmitoylation is catalysed by palmitoyl-proteins thioesterases (PPTs), acyl protein thioesterases, and the α/β hydrolase domain-containing proteins [11, 12].

A substantial number of synaptic receptors are palmitoylated. The glutamate ionic receptors, AMPAR and NMDAR, are major postsynaptic receptors that mediate excitatory neurotransmission and synaptic plasticity. Palmitoylation of AMPAR, mediated by DHHC2 and DHHC3, is involved in receptor regulation and trafficking[13–15]. Palmitoylation of NMDAR, mediated by DHHC3, leads to retention in the Golgi apparatus, trafficking and membrane localization[16–18].

$GABA_AR$ mediates fast inhibitory neurotransmission. The palmitoylation of γ2 subunit of $GABA_AR$ catalysed by GODZ regulates the $GABA_AR$ clustering and cell surface stability [19, 20], which is required for normal assembly and function of GABAergic inhibitory synapses[21]. Gephyrin is a central element

that anchors, clusters, and stabilizes glycine and $GABA_AR$ at inhibitory synapses. Gephyrin palmitoylation mediated by DHHC12 potentiates GABAergic synaptic transmission[22].

The role of depalmitoylation on synaptic receptors has not been reported. Previous studies have identified that ABHD17 specifically mediates PSD95 depalmitoylation [23]. PPT1, encoded by *CLN1* gene [1, 11, 24, 25], is a lysosomal enzyme [11] which mediates protein depalmitoylation by removing the palmitate residues from the S-acylated proteins [24, 26].

Mutations in *CLN1* gene cause a deficiency in PPT1, which clinically presents as fatal neurodegenerative disorders in the juvenile period, termed as neuronal ceroid lipofuscinosis (NCL), the most common type of recessively inherited childhood encephalopathies. Infantile neuronal ceroid lipofuscinosis (INCL) is the most severe form of NCL. Children with INCL are normal at birth but undergo retinal degeneration leading to blindness, impairment of learning and memory, and seizures[27–31].

PPT1 plays critical roles in neuronal transmission by mediating vesicle refill in presynaptic terminals; therefore, PPT1 deficiency causes abnormal and persistent membrane accumulation of synaptic vesicle proteins, such as vesicle-associated membrane protein 2 and syntaxin-1[5]. A recent study indicates that PPT1 knockout (KO) mice showed impaired long-term potentiation in the hippocampus in response to tetanic stimulation[32]. $CLN3^{-/-}$ hippocampus showed progressive network hyperexcitability progressively with altered hippocampal network activity[33]. However, the molecule mechanism by which PPT1 manipulates synaptic signaling remains elusive. Whether the key postsynaptic receptors, such as AMPAR and $GABA_AR$, are substrates of PPT1 and how these substrates modulate synaptic function remains unclear. Uncovering the roles of PPT1 in synaptic receptors could elucidate the physiological functions of PPT1 in learning and memory.

Materials And Methods

Animals

The strategy of point mutation of the *CLN1* gene to generate PPT-KI mice (*Cln1* c.451C>T (p.R151X)) is shown in **Fig. S1**. C57BL/6N mice were purchased from Beijing Vital River Laboratory Animal Technology Co., Ltd (animal license number: 2016-0006) and were used as the wildtype (wildtype) controls. All animals were housed and maintained in the specific pathogen-free animal facility of Animal Experiment Center of the Institute of Psychiatry and Neuroscience of Xinxiang Medical University (XXMU) with a 12-h light/dark cycle. Animals had *ad libitum* access to food and water, except during food or water deprivation. A previous study demonstrated that BuHA can easily pass the blood-brain barrier in the mouse brain [34]. PPT1-KI mice and their littermates were orally administrated with 1 mM BuHA for 3 months before mating. After pregnancy, the young mice took food and water (containg 1 mM BuHA) freely during the whole period. All efforts were made to minimize animal suffering and reduce the number of animals used. All reagents were purchased from Sigma-Aldrich (St. Louis, MO) unless otherwise stated.

Electrophysiology

In vivo electrophysiological recording

Stereotaxic surgery, electrode implantation and signal acquisition

Mice were deeply anesthetized with an intraperitoneal injection of 1% pentobarbital sodium (0.45 mL~0.5 mL/100g). Under anesthesia, mice were secured in a stereotaxic frame with ear bars. The head was shaved with a razor, and a midline 5-mm incision was made with a sterile scalpel. The subcutaneous tissue was removed from the skull, a craniotomy (~1.5 x 0.5 mm) was drilled (AP: 1.82 mm, ML:1.25 mm, DV:1.5 mm, right hemisphere) at CA1 region. Two steel screws were anchored at the anterior and posterior edges of the surgical site to secure the implant in place. After endocranium was removed, a 4*2 micro wire electrode (KD-MWA-8, 25 μm nitinol wire, Kedou (Suzhou) Brain-Computer Technology Co., Ltd.) with 3 μm polyethylene glycol coating was implanted into pyramidal cell layer of CA1. The craniotomy site was then sealed with a sterile silicone elastomer (Kwik-Sil WPI) to alleviate brain injury. After surgery, the implanted electrodes and screws were cemented integrally to the skull using denture base resin type II (Shanghai Medical Instruments Co., LTD.). After surgery, animals were housed individually on a reversed 12/12 hr day/night schedule.

Following one week of recovery, wideband signals were recorded using OmniPlex Neural Recording Data Acquisition System (Plexon Inc., Dallas, TX, USA) with 8 kHz global low-pass filter. Continue spike was sampled at 4 kHz following with 300 Hz low-cut filter. Field potential (FP) was set at 200 low-pass filter and down-sampled to 1 kHz. After recording, the hippocampus was post-fixed to perform Nissl stain in order to verify the proper placement of the electrodes in the target region.

Spikes were sorted with the Offline Sorter (Plexon Inc., Dallas, TX, USA) to classify the electric activity of individual neurons, based on the first to third principal components[35]. Spike units were excluded using Remove Short ISI Waveform Tools when the absolute refractory period of single unit autocorrelation was < 1 ms. Cross-channel artifacts identified by their time-concidence across channels were also invalidated.

The power spectrum density and spectrogram of continuous filed potential (FP) were computed using NeuroExplorer (Nex Technologies, Colorado Springs, CO, USA) with 1024 frequency values and 25% window overlap. Before this process, FP signal values were multiplied by the coefficients of the Hann window, and discrete fast Fourier transformations of the results were calculated using formulas defined previously[36]. gamma waves were filtered by band-pass filtering of FP data using NeuroExplorer software with Digital Filtering of Continuous Variables function. The valley of γ wave timestamp was identified as a reference event using Find Oscillation function for plotting perievent raster.

In vitro electrophysical recording

Slice preparation

The mice were anesthetized with urethane and perfused with ice-cold artificial cerebrospinal fluid (aCSF) through the left ventricle until the limbs turned white. The brain was then rapidly removed and immersed in ice-cold aCSF containing 225 mM sucrose, 3 mM KCl, 6 mM $MgCl_2$, 1.25 mM NaH_2PO_4, 24 mM $NaHCO_3$, 0.5 mM $CaCl_2$, 10 mM glucose. Transverse slices (350 μM thickness) were prepared using a vibratome (Ci-7000SMZ2, Campden instrument, Loughborough, UK). Immediately after preparation, slices were transferred to a nylon net within a chamber, and two sides of the chamber were exposed to normal aCSF containing mM 126 NaCl, 3 mM KCl, 1.25 mM NaH_2PO_4, 2 mM $MgSO_4$, 24 mM $NaHCO_3$, 2 mM $CaCl_2$, and 10 mM glucose, bubbled with a mixture of 95 % O_2 and 5 % CO_2, and kept at pH 7.35-7.45 at room temperature (RT) for storage or 32 °C for recording. The perfusion rate was maintained at 1-2 mL/min [37].

Patch clamp recording

Miniature inhibitory post synaptic currents (mIPSCs) were measured in voltage-clamp mode at -70 mV in the presence of metabotropic glutamate receptors blocker, [250 μM (S)-α-methyl-4-carboxyphenylglycine (MCPG)], a glycine receptor blocker (1 μM strychnine), and $GABA_B$ receptor blocker (1 μM CGP55845)[38]. The pipette solution contained 140 mM CsCl, 10 mM Na-HEPES, 10 mM EGTA, 2 mM Mg-ATP and 5 mM QX-314 (pH 7.3). To block EPSCs, 25 μM D-(−)-2-amino-5-phosphonopentanoic acid (D-APV) and 5 μM 6-cyano-7-nitroquinoxaline-2,3-dione (CNQX) were added in the bath solution just before used[39, 40]. For evoked IPSCs recordings, the cells were clamped at +40 mV[41]. All patch-clamp recordings were performed at RT.

To isolate AMPAR-mediated miniature excitatory postsynaptic currents (mEPSCs), 1 μM tetrodotoxin, 10 μM D-APV, 10 μM bicuculline, and 10 μM strychnine were added to the bath solution. Pipette (3-4 MΩ) solution contained 125 mM Cs-gluconate, 20 mM KCl, 4 mM Mg-ATP, 10 mM Na_2-phosphocreatine, 0.3 mM Na_2-GTP, 10 mM HEPES, 0.5 mM EGTA, and 5 mM QX314 (pH 7.3) adjusted with CsOH. For evoked EPSCs recording, neurons were voltage-clamped at -70 mV to record AMPAR- mediated EPSCs or at +40 mV to record dual-component EPSCs containing NMDAR-mediated EPSCs. AMPAR/NMDAR ratios were also calculated by dividing the peak of the AMPAR-mediated EPSC at -70 mV by the value of the NMDAR-mediated EPSC after a stimulation start time 50 ms at +40 mV. For current clamp recording, a K-gluconate-based intercellular solution were used, and cells were clamped at their resting potentials. A 300-pA current was injected into the cell to induce action potential by bath application with 10 μM CNQX, 5 μM L-AP5, 10 μM bicuculline and 10 μM strychnine.

Currents were amplified with a Multiclamp 700B amplifier (Molecular Devices, Sunnyvale, CA), low-pass filtered at 1 kHz, and digitised with a Digidata 1550B interface (Molecular Devices) at 5 kHz. The detection and analysis of synaptic currents were conducted using pClamp 10 software (Molecular Devices). Offline analysis of mEPSCs/IPSCs was performed using Clampfit 10.4.2.0 (Molecular Devices) software. Only recordings where series resistance remained below 16 MΩ and did not increase by more than 20 % during the experiment were included in the analysis[40].

Acyl biotin exchange (ABE) assay

ABE was performed as previously described [13, 17, 42]. Briefly, the lysates were incubated with 10 mM N-ethylmaleimide (NEM, E3876; Sigma) overnight at 4 °C. Then, NEM was removed by three sequential chloroform/methanol (CM) precipitations. After three CM precipitations, proteins were solubilized in solubilizing buffer with 1 M hydroxylamine hydrochloride (159417, Sigma), 1 mM HPDP-Biotin (A8008; APExBIO, Houston, TX), 0.2 % TritonX-100 (T8787, Sigma), and protease inhibitors (4693132001; Roche, Basel, Switzerland) in phosphate-buffered saline (pH 7.4). After incubation for 1 h at RT, proteins were precipitated by CM and then suspended with 200 μM HPDP-biotin and 0.2 % Triton X-100 for 1.5-2 h at RT. After 3 CM precipitations, the proteins were incubated with streptavidin-agarose (16-126; Millipore sigma, Burlington, MA) for one night at 4 °C. The beads were washed five times with wash buffer containing 150 mM NaCl, 50 mM Tris-HCl, 5 mM EDTA (pH 7.4), and 0.2 % Triton X-100. After washing, the proteins were eluted with wash buffer containing 1.5 % β-mercaptoethanol (Sigma-Aldrich, M3148) at 37 °C for 0.5 h with agitation (350 rpm), and then heated in a 100 °C water bath for 10 min. After centrifugation, the released proteins in the supernatant were denatured in sodium dodecyl sulfate sample buffer and processed for Western blotting with primary antibody ABE assays; all other biochemical experiments were performed at least three times. In each case, a representative experiment is presented.

The possible palmitoylation sites (C165, C179, C260, C319) of GABAAR α1 subunit was forecasted by CSS-Palm Online Service webset. All the mutants (GABAARα1 C165A, C179A, C165/179A) were purchased from Fenghui Biology (Hu'nan, China). ABE assay was performed as mentioned above.

Other experimental procedures are provided in the **Supplementary Information**:

S1 Behavioral studies

Morris water maze (MWM)

Y maze

S2 Biochemical analysis

Cell membrane/cytoplasmic protein extraction

Co-immunoprecipitation (Co-IP)

Quantitative polymerase chain reaction (qPCR)

Cell culture

Statistical analysis

All data were acquired and analyzed by experimenters who were blinded with respect to the genotype of the mice and acute slices. All data were analysed using the SPSS Statistics 20 (IBM, Armonk, NY). We

confirmed homogeneity of variances by the Levene's test and equality of mean by the Brown-Forsythe test. Electrophysiology data were analysed using t-test for two group comparisons and one-way ANOVA test for multi-group comparisons. Western blot results were analysed by t-test for two group comparisons and one-way ANOVA test for multi-group comparisons.

Results

GABA $_A$ R subunits are dynamically regulated at different stages of the age in PPT1-KI mice.

Initially, we investigated $GABA_AR$ α1, β2, and γ2 subunits expression at different stages of ages (Fig. 1a). α1 subunit represented dynamically overload on the cellular surface (Fig. 1b). Compared with wildtype littermates, membrane expression of $GABA_AR$ α1 subunit was increased at age of 1–2 months (*P< 0.05), the increasing tendency was reversed at 6 months, but decreased at 7 months (*P< 0.05). While membrane expression of β2 and γ2 subunits had no significant difference (Fig. 1b**2, b3)** compared with wildtype group. qPCR results showed that mRNA expression of $GABA_AR$ subunits have no significant difference until 7-months-old age (*P< 0.05) **(Fig. S2 a-c)**, indicating that the membrane overload of $GABA_AR$ occurred in the process of post-translational modification.

We focused on PPT1-KI mice at 1-to 2-months-old. Immunofluorescence double staining showed that colocalization of $GABA_AR$ and gephyrin was increased in CA1, CA3 and CA4 areas **(Fig. 2c1-c3)**, indicating increased expression of $GABA_AR$ at the postsynaptic membrane. Western blot analysis showed that the expression level of $GABA_AR$ on the cellular membrane in PPT1-KI mice were significantly higher than that of wildtype group, which could be reduced by *in vitro* incubation with different concentrations of BuHA (1, 5, 25 mM) (*P< 0.05, n = 3 for each group) **(Fig. 2d1, d2)**.

These results indicated that the distribution of $GABA_AR$ α1 subunit on the membrane surface was dramatically upregulated in young PPT1-KI hippocampus.

Ppt1-ki Selectively Induces Gabar Hyperpalmitoylation With Increased Gabar Membrane Expression And Disrupted Gabaergic Neurotransmission

We performed ABE experiments using membrane fractions and confirmed that both $GABA_AR$ and gephyrin, the specific postsynaptic scaffold protein of $GABA_AR$, were palmitoylated **(Fig. 2a1, d1)**. Bioinformtics predicted that there are several cysteine residues (C260, C319, C165, and C179) which may be palmitoylated. Mutating the evolutionarily conserved 260-cysteine residue to alanine, singly (C260A) or in combination (C260/319A) could markedly block palmitoylation (Fig. 2b), suggesting that C260 is required for $GABA_AR$ palmitoylation. We did not observe significant changes of C165 and C179 mutants,

suggesting that both of 165 and 179 cysteine residues were not the modulation sites for $GABA_AR$ palmitoylation.

ABE experimental results showed that PPT1 deficiency upregulated $GABA_AR$ palmitoylation (*P< 0.05) **(Fig. 2c1-c2)**, without affecting gephyrin palmitoylation **(Fig. 2d1-d2)**. *In vitro* incubation with BuHA suppressed PPT1-KI induced $GABA_AR$ hyperpalmitoylation (1mM: n.s.; 5mM: *P< 0.05; 25mM: **P< 0.01). *In vitro* co-immunoprecipitation experiments further identified the interaction between PPT1 and $GABA_AR$ **(**Fig. 2e**)**, indicating that $GABA_AR$ is a substrate of PPT1.

To determine the role of depalmitoylation on GABAergic neurotransmission, we recorded evoked IPSCs by holding the pyramidal cell in CA1 at + 40 mV, as shown in Fig. 3a. In contrast to wildtype neurons, PPT1-KI neurons had an increased amplitude (*P< 0.05) **(**Fig. 3b**)** and a decremental fast tau (*P= 0.035) without affecting the slow tau by the double exponential fitting repolarization phase **(Fig. 3c1-c2)**. We also pharmacologically isolated mIPSCs by patching pyramidal cell in CA1, which were abolished by bicuculline, and confirmed that these are GABA-mediated currents **(**Fig. 3d**)**. PPT1-KI neurons had both increased mIPSCs amplitudes and frequencies. Next, we treated hippocampal slices with BuHA. Both the amplitude and frequency of mIPSCs recorded from hippocampal slices in PPT1-KI mice treated with BuHA was significantly recovered compared to vehicle-treated slices (amplitude: wildtype vs PPT1-KI, ***P< 0.001; PPT1-KI vs PPT1-KI + BuHA, *P= 0.049; frequency: wildtype vs PPT1-KI, ***P< 0.001; PPT1-KI vs PPT1-KI + BuHA, **P= 0.01) **(**Fig. 3e-f**)**. These results demonstrated that deficiency of $GABA_AR$ depalmitoylation caused aberrant GABAergic neurotransmission.

We also investigated whether PPT1 could also regulate the palmitoylation of ionotropic glutamate receptors (iGluRs). ABE results showed that the palmitoylation states of AMPAR **(Fig. S3a)**, NMDA-2a/2b **(Fig. S3b-c)**, PSD95/93[23] **(Fig. S3d-e)** and SAP102 **(Fig. S3g)** were comparable between PPT1-KI and wildtype mice, suggesting that these proteins are not efficient substrates of PPT1.

To determine whether PPT1 mediated glutamatergic neurotransmission, we recorded mEPSCs by patching pyramidal neurons in the hippocampal CA1 region. Both amplitude and frequency of mEPSCs were comparable between PPT1-KI and wildtype mice **(Fig. S4a-b)**. We also recorded evoked EPSCs at + 40 mV. The hippocampal neurons from PPT1-KI mice showed slightly enhanced AMPAR-mediated EPSCs **(Fig. S4c-d1)**, but there was no difference in NMDAR-mediated EPSCs **(Fig. S4d2)** or AMPA/NMDA current ratio **(Fig. S4d3)** compared with those of wildtype mice. Western blot analysis showed that the distribution of AMPAR, NMDAR-2a/2b and scaffold proteins (PSD95/93 and SAP102) on the cellular surface of hippocampal neurons were comparable between wildtype and PPT1-KI mice **(Fig. S4e-f)**. These data suggest that PPT1-KI does not significantly affect glutamatergic expression and transmission.

PPT1 deficiency impairs neural network oscillations.

Previous study reported that *CLN3-/-* mice have a decrease in relative power of δ frequency band with a trend toward increased power of β and γ bands[33]. We conducted *in vivo* electrophysiological recording from hippocampal CA1 region of young PPT1-KI mice at 1-to 2-months-old. Power spectrum analysis showed that PPT1 deficiency mice had an increased power at γ frequency band (30–800 Hz) (***P< 0.001) (Fig. 4a-d), while phase coupling analysis showed decreased spike-phase coupling in hippocampal CA1 of PPT1-KI mice (*P< 0.05, **P< 0.01) compared to wildtype mice under free-moving condition, which were partly recovered by oral administration with BuHA (Fig. 5a-g).These results indicate that hyperpalmitoylation of $GABA_AR$ abnormally enhances γ band oscillation with the disruption of the temporal relationships between neuronal firing and γ rhythms.

PPT1 lost function mutation knock-in impairs learning and memory deficits in mice.

We also demonstrated that PPT1-KI mice began to suffer from impaired spatial learning and memory at as early as 2 months of age. As shown in Fig. 6a, *post hoc* comparisons revealed that PPT1-KI mice took more time to find the hidden platform and spent less times in the target area entrance on training days 2–5 compared with wildtype littermates. Oral administration of 1 mM BuHA, a thioesterase mimetic that selectively cleaves thioester linkage in palmitoylated proteins and compensates for the molecular defect caused by PPT1 mutations[34], improved spatial learning compared to untreated PPT1-KI mice (*P< 0.05, **P< 0.01, ***P< 0.001) (Fig. 6a-b). The swimming distance and speed used by the PPT1-KI and wildtype mice to locate the submerged escape platform over the 5 days of testing were not significantly difference (Fig. 6d-e). On the test day (day 6), as shown in Fig. 2e, PPT1-KI mice entered the target arena fewer times (wildtype vs. PPT1-KI, **P= 0.007; PPT1-KI vs. PPT1-KI + BuHA, **P= 0.005) (Fig. 6f) and had an increased swimming distance beyond the target arena. Times to cross the targe area was also decreased compared to wildtype, which could be recovered by BuHA treatment (wildtype vs. PPT1-KI: ***P< 0.001; PPT1-KI vs. PPT1-KI + BuHA: **P< 0.01) (Fig. 6g). Y-maze experiments showed that PPT1-KI mice spent less time in the novel arm zone (*P= 0.0429) (Fig. 6h-i), while the total distance (Fig. 6j) and entries in novel zone (Fig. 6k) were not different. These results indicate that PPT1-KI mediated depalmitoylation deficit impairs learning and memory formation.

Discussion

$GABA_AR$, but not iGluRs, is the substrate of PPT1

Numerous studies have demonstrated that both $GABA_AR$[19–21] and gephyrin[22, 43] are palmitoylated proteins. Palmitoylation regulates the clustering and cell surface stability of $GABA_AR$[19]. Here, our study demonstrated $GABA_AR$ α1 subunit is the substrate of PPT1, indicating that $GABA_AR$ depalmitoylation is mediated by PPT1. PPT1 deficiency results in the retention of $GABA_AR$ on the cellular membrane, which may lead to aberrant inhibitory GABAergic transmission and disrupted neuronal network oscillation. A previous study has demonstrated enhanced vulnerability to NMDA-induced excitotoxicity in $PPT1^{-/-}$ cultured neurons, reflecting the predominance of GluN2b-containing receptors in these neurons[44]. We

did not find that PPT1 deficiency caused the retention of iGluRs or their scaffold proteins on the membranes of hippocampal neurons of PPT1-KI mice at an early stage **(Fig. S4)**. The ABE results imply that the depalmitoylation of excitatory glutamate receptors is not mediated by PPT1. It is also noteworthy that the mRNA expression of ABDH17B, another depalmitoylase in the central nervous system[23, 45–47], is lower in the hippocampi of PPT1-KI mice **(Fig. S3i)**. Currently, we have no clear explanation of this result, which remains to be further studied.

PPT1 deficiency abnormally enhances γ oscillation with the disruption of γ phase coupling.

Numerous studies have shown that γ oscillation are modulated by a variety of cognitive processes such as attention, object recognition, and working memory[48–51]. Therefore, γ activity is assumed to reflect an integration mechanisms of the brain and related to advanced cognitive function[52], such as memory encoding.

A recent study reported that SMAD3 deficiency inhibits long-term potentiation induction by enhancing phasic and tonic GABAAR-mediated neurotransmission[53]. γ phase locking of spikes of pyramidal cells was impaired in amyloid precursor protein knock-in mice[54]. In terms of our *in vivo* electrophysiological results, both of hippocampal low and high γ oscillation recorded from PPT1-KI mice were enhanced compared with their wildtype littermates. However, phase-locking analysis showed that more PPT1-KI neurons lost γ phase-locking as shown in Fig. 5. In consideration of a bad performance PPT1-KI mice had in behavior test, we conclude that the hyperpalmitoylation of $GABA_AR$ breakouts the balance between excitation and inhibition, disrupts the γ phase-locking in PPT1-KI hippocampus and impairs memory formation. A previous study demonstrated that PPT1-KO mice exhibit excitotoxicity in glutamatergic neurons due to changes in the NMDA2a/2b ratio[44]. However, there was no change in the expressional profile of GluA1, GluN2A, or GluN2B in PPT1-KI mice at an early age, suggesting that the impaired memory formation is less likely to be associated with iGluRs expression.

Our results show that inhibitory GABAergic neuronal transmission is dysregulated in PPT1-KI mice, which presented as increased amplitude and frequency of mIPSCs, increased amplitude of evoked IPSCs, and increased $GABA_AR$ in postsynaptic membrane in this study. A recent study reported that SMAD3 deficiency inhibits LTP induction by enhancing phasic and tonic $GABA_AR$-mediated neurotransmission[53]. Our study reveals the critical role of PPT1 in the regulation of $GABA_AR$ depalmitoylation which contributes to synaptic function, learning, and memory.

A previous study indicated that older *Cln1*$^{-/-}$ mice (~ 5–6 months old) exhibited impairments in spatial learning and memory, but the young *Cln1*$^{-/-}$ mice only had disorders of motor/sensorimotor function[55]. In PPT1-KI mice, we found that the early impairment of learning and memory is correlated with the enhancement of γ oscillation with the disruption of phase-locking.

Assuming that PPT1 deficiency-induced chaos of network oscillation mediates memory decline in PPT1-KI mice, we rescued memory deficits in PPT1-KI mice by treating them with BuHA, suggesting that the

cognitive decline in PPT1-KI mice is pharmacologically treatable at least at this stage of disease progression in mice.

In summary, PPT1 deficiency caused $GABA_AR$ hyperpalmitolation and membrane retention as well as increased activity of GABAergic neurons, which may result in upregulated $GABA_AR$-mediated inhibition and reduced excitation of pyramidal neurons, neuronal network oscillations, and learning and memory in young PPT1-KI mice. Since the altered GABAergic neurotransmission is thought to produce hippocampal cognitive dysfunction in Alzheimer's disease, early correction of PPT1 deficiency and thus abnormal GABAergic inhibition may be critical for the intervention not only for INCL but also for other neurodegenerative disorders.

Abbreviations

ABE
acyl biotin exchange
AMPAR
α-amino-3-hydroxy-5-methyl-4-isoxazole-propionic acid receptor
APTs
acyl protein thioesterases
BuHA
N-tert-Butylhydroxylamine hydrochloride
CGP55845
(2S)-3-[[(1S)-1-(3,4-dichlorophenyl)ethyl]amino-2hydroxypropyl] (phenylmethyl) phosphinic acid
CNQX
6-cyano-7-nitroquinoxaline-2,3-dione
D-APV
D-(−)-2-amino-5-phosphonopentanoic acid
EPSC
excitatory postsynaptic current
$GABA_AR$
γ-aminobutyric acid A receptor
IPSC
inhibitory post synaptic currents
LFP
local field potential
MCPG
(S)-α-methyl-4-carboxyphenylglycine
MWM
morris water maze
NCLs

neuronal ceroid lipofuscinosis
NMDAR
N-methyl-d-aspartic acid receptor
PPT1
palmitoyl-protein thioesterase 1
TTX
tetrodotoxin
ZDHHCs
Asp-His-His-Cys

Declarations

Funding

This work was supported by funds from the National Natural Science Foundation (CBL, No.: 81771517) and the Open Project Program of the Third Affiliated Hospital of Xinxiang Medical University (No. KFKTYB202111).

Competing Interests

The authors declare no competing interests.

Authors' contributions

S.Y.P., J.T., and C.B.L. designed research; S.Y.P., J.T., and C.B.L. conducted review and editing; J.T., J.J.G., X.Z., X.S.Z., B.Y.F, J.M.L., Y.W.Q., T.G.Y., Q.Y.Z., C.B.L., and S.Y.P. performed the experiments or analyses of the data; S.Y.P. provided funding acquisition, project administration, and resources; and S.Y.P., J.T., and C.B.L. wrote the paper. All authors read and approved the final manuscript.

Availability of data and materials

Raw data were generated at the Institute of Psychiatry and Neuroscience of Xinxiang Medical University. The derived data supporting the findings of this study are available from the corresponding author upon request.

Ethics approval

Animal use and procedures were performed according to the regulations and requirements of XXMU Animal Ethics Committee (No. XYLL2021053).

Acknowledgments

We thank Prof. Jianzhi Wang for her critical review of the manuscript and helpful suggestions.

References

1. Camp LA, Verkruyse LA, Afendis SJ, Slaughter CA, Hofmann SL: **Molecular cloning and expression of palmitoyl-protein thioesterase**. *The Journal of biological chemistry* 1994, **269**(37):23212-23219.
2. Linder ME, Deschenes RJ: **Palmitoylation: policing protein stability and traffic**. *Nature reviews Molecular cell biology* 2007, **8**(1):74-84.
3. Resh MD: **Palmitoylation of ligands, receptors, and intracellular signaling molecules**. *Science's STKE : signal transduction knowledge environment* 2006, **2006**(359):re14.
4. Smotrys JE, Linder ME: **Palmitoylation of intracellular signaling proteins: regulation and function**. *Annual review of biochemistry* 2004, **73**:559-587.
5. Kim SJ, Zhang Z, Sarkar C, Tsai PC, Lee YC, Dye L, Mukherjee AB: **Palmitoyl protein thioesterase-1 deficiency impairs synaptic vesicle recycling at nerve terminals, contributing to neuropathology in humans and mice**. *The Journal of clinical investigation* 2008, **118**(9):3075-3086.
6. Aicart-Ramos C, Valero RA, Rodriguez-Crespo I: **Protein palmitoylation and subcellular trafficking**. *Biochimica et biophysica acta* 2011, **1808**(12):2981-2994.
7. Ji B, Skup M: **Roles of palmitoylation in structural long-term synaptic plasticity**. *Molecular brain* 2021, **14**(1):8.
8. Jin J, Zhi X, Wang X, Meng D: **Protein palmitoylation and its pathophysiological relevance**. *Journal of cellular physiology* 2021, **236**(5):3220-3233.
9. Lemonidis K, Werno MW, Greaves J, Diez-Ardanuy C, Sanchez-Perez MC, Salaun C, Thomson DM, Chamberlain LH: **The zDHHC family of S-acyltransferases**. *Biochemical Society transactions* 2015, **43**(2):217-221.
10. Mitchell DA, Vasudevan A, Linder ME, Deschenes RJ: **Protein palmitoylation by a family of DHHC protein S-acyltransferases**. *Journal of lipid research* 2006, **47**(6):1118-1127.
11. Vesa J, Hellsten E, Verkruyse LA, Camp LA, Rapola J, Santavuori P, Hofmann SL, Peltonen L: **Mutations in the palmitoyl protein thioesterase gene causing infantile neuronal ceroid lipofuscinosis**. *Nature* 1995, **376**(6541):584-587.
12. Lin DT, Conibear E: **Enzymatic protein depalmitoylation by acyl protein thioesterases**. *Biochemical Society transactions* 2015, **43**(2):193-198.
13. Hayashi T, Rumbaugh G, Huganir RL: **Differential regulation of AMPA receptor subunit trafficking by palmitoylation of two distinct sites**. *Neuron* 2005, **47**(5):709-723.
14. Yang G, Xiong W, Kojic L, Cynader MS: **Subunit-selective palmitoylation regulates the intracellular trafficking of AMPA receptor**. *The European journal of neuroscience* 2009, **30**(1):35-46.
15. Noritake J, Fukata Y, Iwanaga T, Hosomi N, Tsutsumi R, Matsuda N, Tani H, Iwanari H, Mochizuki Y, Kodama T *et al*: **Mobile DHHC palmitoylating enzyme mediates activity-sensitive synaptic targeting of PSD-95**. *The Journal of cell biology* 2009, **186**(1):147-160.
16. Kang R, Wan J, Arstikaitis P, Takahashi H, Huang K, Bailey AO, Thompson JX, Roth AF, Drisdel RC, Mastro R *et al*: **Neural palmitoyl-proteomics reveals dynamic synaptic palmitoylation**. *Nature* 2008,

456(7224):904-909.

17. Hayashi T, Thomas GM, Huganir RL: **Dual palmitoylation of NR2 subunits regulates NMDA receptor trafficking**. *Neuron* 2009, **64**(2):213-226.
18. Mattison HA, Hayashi T, Barria A: **Palmitoylation at two cysteine clusters on the C-terminus of GluN2A and GluN2B differentially control synaptic targeting of NMDA receptors**. *PloS one* 2012, **7**(11):e49089.
19. Rathenberg J, Kittler JT, Moss SJ: **Palmitoylation regulates the clustering and cell surface stability of GABAA receptors**. *Molecular and cellular neurosciences* 2004, **26**(2):251-257.
20. Keller CA, Yuan X, Panzanelli P, Martin ML, Alldred M, Sassoè-Pognetto M, Lüscher B: **The gamma2 subunit of GABA(A) receptors is a substrate for palmitoylation by GODZ**. *The Journal of neuroscience : the official journal of the Society for Neuroscience* 2004, **24**(26):5881-5891.
21. Fang C, Deng L, Keller CA, Fukata M, Fukata Y, Chen G, Lüscher B: **GODZ-mediated palmitoylation of GABA(A) receptors is required for normal assembly and function of GABAergic inhibitory synapses**. *The Journal of neuroscience : the official journal of the Society for Neuroscience* 2006, **26**(49):12758-12768.
22. Dejanovic B, Semtner M, Ebert S, Lamkemeyer T, Neuser F, Lüscher B, Meier JC, Schwarz G: **Palmitoylation of gephyrin controls receptor clustering and plasticity of GABAergic synapses**. *PLoS biology* 2014, **12**(7):e1001908.
23. Yokoi N, Fukata Y, Sekiya A, Murakami T, Kobayashi K, Fukata M: **Identification of PSD-95 Depalmitoylating Enzymes**. *The Journal of neuroscience : the official journal of the Society for Neuroscience* 2016, **36**(24):6431-6444.
24. Camp LA, Hofmann SL: **Purification and properties of a palmitoyl-protein thioesterase that cleaves palmitate from H-Ras**. *The Journal of biological chemistry* 1993, **268**(30):22566-22574.
25. Jalanko A, Braulke T: **Neuronal ceroid lipofuscinoses**. *Biochimica et biophysica acta* 2009, **1793**(4):697-709.
26. Lu JY, Hofmann SL: **Thematic review series: lipid posttranslational modifications. Lysosomal metabolism of lipid-modified proteins**. *Journal of lipid research* 2006, **47**(7):1352-1357.
27. Hobert JA, Dawson G: **Neuronal ceroid lipofuscinoses therapeutic strategies: past, present and future**. *Biochimica et biophysica acta* 2006, **1762**(10):945-953.
28. Haltia M: **The neuronal ceroid-lipofuscinoses: from past to present**. *Biochimica et biophysica acta* 2006, **1762**(10):850-856.
29. Mukherjee AB, Appu AP, Sadhukhan T, Casey S, Mondal A, Zhang Z, Bagh MB: **Emerging new roles of the lysosome and neuronal ceroid lipofuscinoses**. *Molecular neurodegeneration* 2019, **14**(1):4.
30. Goebel HH, Wisniewski KE: **Current state of clinical and morphological features in human NCL**. *Brain pathology (Zurich, Switzerland)* 2004, **14**(1):61-69.
31. Mole SE: **The genetic spectrum of human neuronal ceroid-lipofuscinoses**. *Brain pathology (Zurich, Switzerland)* 2004, **14**(1):70-76.

32. Matt L, Kim K, Chowdhury D, Hell JW: **Role of Palmitoylation of Postsynaptic Proteins in Promoting Synaptic Plasticity**. *Frontiers in molecular neuroscience* 2019, **12**:8.
33. Ahrens-Nicklas RC, Tecedor L, Hall AF, Lysenko E, Cohen AS, Davidson BL, Marsh ED: **Neuronal network dysfunction precedes storage and neurodegeneration in a lysosomal storage disorder**. *JCI insight* 2019, **4**(21).
34. Sarkar C, Chandra G, Peng S, Zhang Z, Liu A, Mukherjee AB: **Neuroprotection and lifespan extension in Ppt1(-/-) mice by NtBuHA: therapeutic implications for INCL**. *Nature neuroscience* 2013, **16**(11):1608-1617.
35. Adamos DA, Kosmidis EK, Theophilidis G: **Performance evaluation of PCA-based spike sorting algorithms**. *Computer methods and programs in biomedicine* 2008, **91**(3):232-244.
36. Sfondouris JL, Quebedeaux TM, Holdgraf C, Musto AE: **Combined process automation for large-scale EEG analysis**. *Computers in biology and medicine* 2012, **42**(1):129-134.
37. Guo F, Zhao J, Zhao D, Wang J, Wang X, Feng Z, Vreugdenhil M, Lu C: **Dopamine D4 receptor activation restores CA1 LTP in hippocampal slices from aged mice**. *Aging Cell* 2017, **16**(6):1323-1333.
38. O'Neill N, Sylantyev S: **Spontaneously opening GABA(A) receptors play a significant role in neuronal signal filtering and integration**. *Cell death & disease* 2018, **9**(8):813.
39. Chakrabarti S, Qian M, Krishnan K, Covey DF, Mennerick S, Akk G: **Comparison of Steroid Modulation of Spontaneous Inhibitory Postsynaptic Currents in Cultured Hippocampal Neurons and Steady-State Single-Channel Currents from Heterologously Expressed alpha1beta2gamma2L GABA(A) Receptors**. *Molecular pharmacology* 2016, **89**(4):399-406.
40. Sabanov V, Braat S, D'Andrea L, Willemsen R, Zeidler S, Rooms L, Bagni C, Kooy RF, Balschun D: **Impaired GABAergic inhibition in the hippocampus of Fmr1 knockout mice**. *Neuropharmacology* 2017, **116**:71-81.
41. Kapur A, Pearce RA, Lytton WW, Haberly LB: **GABAA-mediated IPSCs in piriform cortex have fast and slow components with different properties and locations on pyramidal cells**. *Journal of neurophysiology* 1997, **78**(5):2531-2545.
42. Wan J, Roth AF, Bailey AO, Davis NG: **Palmitoylated proteins: purification and identification**. *Nature protocols* 2007, **2**(7):1573-1584.
43. Shen ZC, Wu PF, Wang F, Xia ZX, Deng Q, Nie TL, Zhang SQ, Zheng HL, Liu WH, Lu JJ *et al*: **Gephyrin Palmitoylation in Basolateral Amygdala Mediates the Anxiolytic Action of Benzodiazepine**. *Biological psychiatry* 2019, **85**(3):202-213.
44. Koster KP, Francesconi W, Berton F, Alahmadi S, Srinivas R, Yoshii A: **Developmental NMDA receptor dysregulation in the infantile neuronal ceroid lipofuscinosis mouse model**. *eLife* 2019, **8**.
45. Won SJ, Cheung See Kit M, Martin BR: **Protein depalmitoylases**. *Critical reviews in biochemistry and molecular biology* 2018, **53**(1):83-98.
46. Kanadome T, Yokoi N, Fukata Y, Fukata M: **Systematic Screening of Depalmitoylating Enzymes and Evaluation of Their Activities by the Acyl-PEGyl Exchange Gel-Shift (APEGS) Assay**. *Methods in*

molecular biology (Clifton, NJ) 2019, **2009**:83-98.

47. Lin DT, Conibear E: **ABHD17 proteins are novel protein depalmitoylases that regulate N-Ras palmitate turnover and subcellular localization**. *eLife* 2015, **4**:e11306.
48. Debener S, Herrmann CS, Kranczioch C, Gembris D, Engel AK: **Top-down attentional processing enhances auditory evoked gamma band activity**. *Neuroreport* 2003, **14**(5):683-686.
49. Fries P, Reynolds JH, Rorie AE, Desimone R: **Modulation of oscillatory neuronal synchronization by selective visual attention**. *Science* 2001, **291**(5508):1560-1563.
50. Sharpee TO, Destexhe A, Kawato M, Sekulić V, Skinner FK, Wójcik DK, Chintaluri C, Cserpán D, Somogyvári Z, Kim JK *et al*: **25th Annual Computational Neuroscience Meeting: CNS-2016**. *BMC Neurosci* 2016, **17 Suppl 1**(Suppl 1):54.
51. Tiitinen H, Sinkkonen J, Reinikainen K, Alho K, Lavikainen J, Näätänen R: **Selective attention enhances the auditory 40-Hz transient response in humans**. *Nature* 1993, **364**(6432):59-60.
52. Buzsáki G, Wang XJ: **Mechanisms of gamma oscillations**. *Annual review of neuroscience* 2012, **35**:203-225.
53. Muñoz MD, Antolín-Vallespín M, Tapia-González S, Sánchez-Capelo A: **Smad3 deficiency inhibits dentate gyrus LTP by enhancing GABAA neurotransmission**. *Journal of neurochemistry* 2016, **137**(2):190-199.
54. Nakazono T, Lam TN, Patel AY, Kitazawa M, Saito T, Saido TC, Igarashi KM: **Impaired In Vivo Gamma Oscillations in the Medial Entorhinal Cortex of Knock-in Alzheimer Model**. *Frontiers in systems neuroscience* 2017, **11**:48.
55. Dearborn JT, Harmon SK, Fowler SC, O'Malley KL, Taylor GT, Sands MS, Wozniak DF: **Comprehensive functional characterization of murine infantile Batten disease including Parkinson-like behavior and dopaminergic markers**. *Scientific reports* 2015, **5**:12752.

Figures

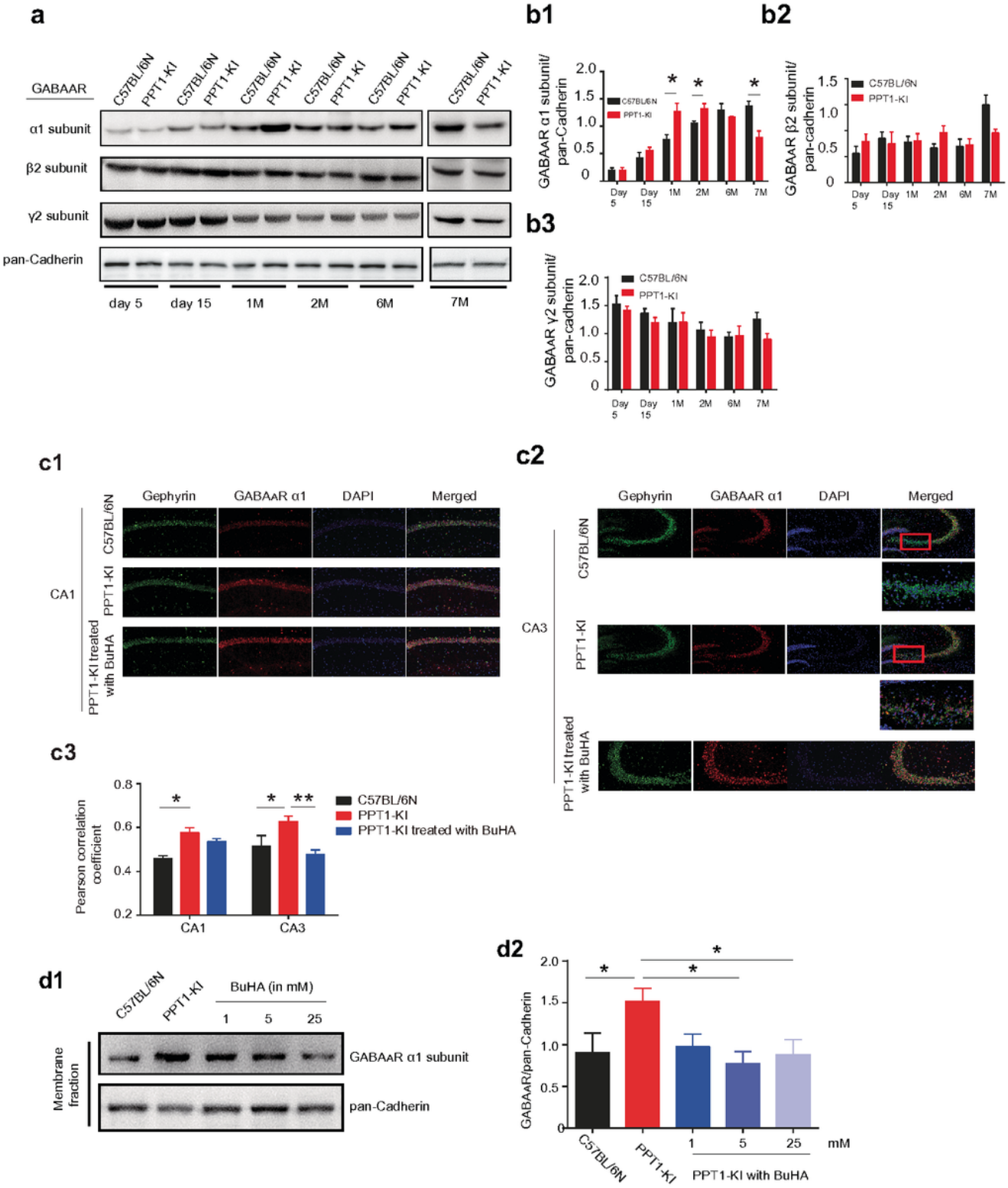

Figure 1

Membrane expression of $GABA_AR$ subunits are dynamically regulated at different stages of the age in PPT1-KI mice.

(a) Comparison of $GABA_AR$ subunits expression by Western blotting analysis of the C57BL/6N and PPT1-KI hippocampal membrane fraction at different stages of the age.

(b1-b3) Bar graph displaying the expression changes of $GABA_AR$ α **(b1)**, β2 **(b2)**, and γ2 **(b3)** subunits at different stages of the age. n=3 for each group, One-way ANOVA test, $*P < 0.05$.

(c1-c3) Colocalization of $GABA_AR$ (red fluorescence) and gephyrin (green fluorescence) at CA1 **(c1)** and CA3 **(c2)** areas of hippocampi from C57BL/6N, PPT1-KI, and PPT1-KI with 1 mM BuHA mice. **(c3)** Pearson's coefficient of $GABA_AR$ and gephyrin in CA1 and CA3 areas. n=4 slices for each group, One-way ANOVA test, $*P < 0.05$, $**P < 0.01$.

(d1, d2) BuHA attenuated PPT1 deficiency-induced $GABA_AR$ overload measured by Western blotting analysis of the hippocampal membrane fraction. One-way ANOVA test, $*P < 0.05$.

Data are represented as mean ± SEM.

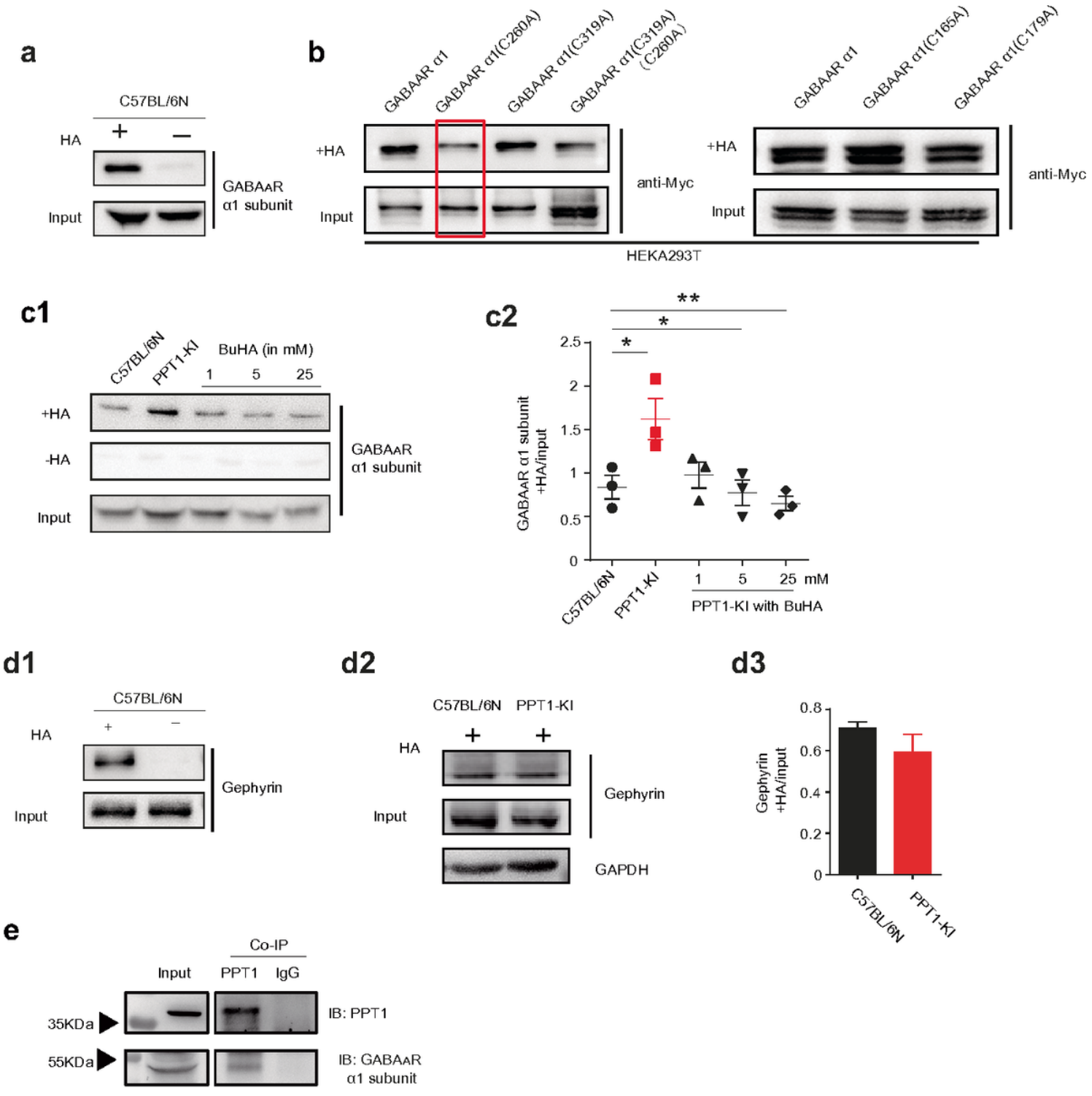

Figure 2

Hyperpalmitoylation of $GABA_AR$ induced by PPT1 deficiency suggests $GABA_AR$ is the substrate of PPT1 enzyme.

(a) Representative immunoblots of palmitoylated $GABA_AR$ α1 subunit using the acyl biotin exchange (ABE) assay in wildtype mice hippocampus.

(b) Mutating C260 could markedly block palmitoylation of $GABA_AR$ α1 subunit in 293T cell line.

(c1, c2) PPT1 deficiency increased level of palmitoylated $GABA_AR$ α1 subunit in the hippocampal extracts of PPT1-KI mice compared with wildtype mice. +HA, with hydroxylamine; n=3, one-way ANOVA test, **P*< 0.05; ***P*<0.01.

(d1) Representative immunoblot of palmitoylated gephyrin measured by using ABE assay in wildtype mice hippocampus.

(d2, d3) PPT1 deficiency did not significantly change the palmitoylated gephyrin level measured by ABE assay. +HA, with hydroxylamine; t-test, **P*< 0.05.

(e) PPT1 palmitoylated $GABA_AR$α1 subunit measured by *in vitro* co-immunoprecipitation. Co-IP, co-immunoprecipitation; IB, Immunoblotting.

Data are represented as mean ± SEM.

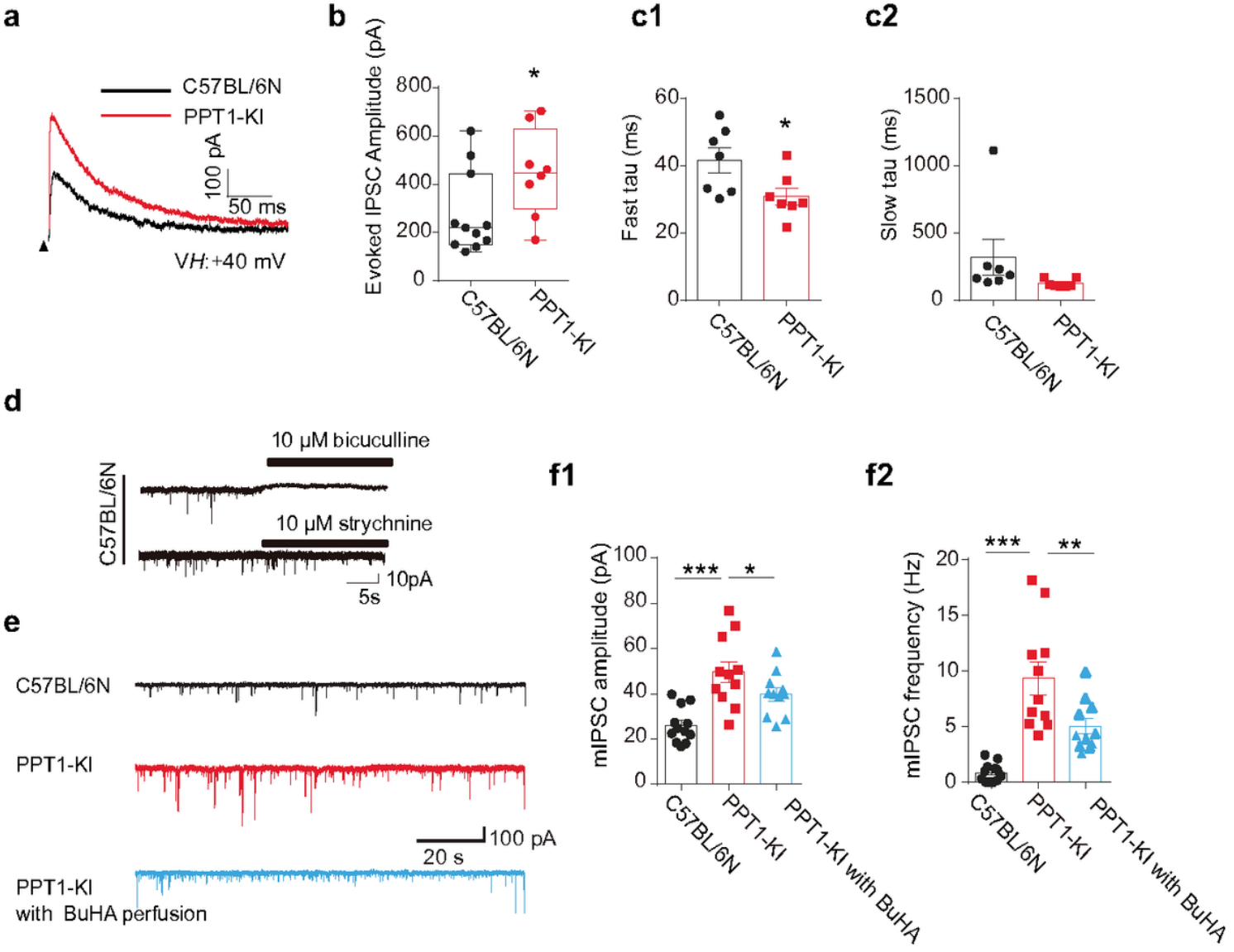

Figure 3

PPT1 deficiency causes abnormal GABAergic transmission.

(a) Representative traces displayed evoked inhibitory postsynaptic currents (IPSCs) recorded at +40 mV from CA1 pyramidal cells of C57BL/6N (black trace) and PPT1-KI mice (red trace).

(b, c) Statistical results of amplitude **(b)**, fast tau **(c1)**, and slow tau **(c2)** from evoked recordings of wildtype (wildtype) and PPT1-KI neurons.

(d) Representative traces displayed miniature IPSCs (mIPSCs) recorded from CA1 pyramidal neurons from C57BL/6N mice, which could be blocked by 10 μM bicuculline (upper trace) and 10 μM strychnine (under trace).

(e) Representative traces displayed mIPSCs recorded from CA1 pyramidal neurons from C57BL/6N (upper trace), PPT1-KI mice (middle trace) and PPT1-KI slices perfused with 1 mM BuHA (under trace). Scale bar: 10 pA, 5 s.

(f1, f2) Histogram showed that both amplitude **(f1)** and frequency **(f2)** of mIPSCs recorded from the PPT1-KI group were increased compared to the wildtype group, which could be recovered by perfusion with 1 mM BuHA. One-way ANOVA test, *P< 0.05, **P< 0.01, ***P< 0.001.

Data are represented as mean ± SEM.

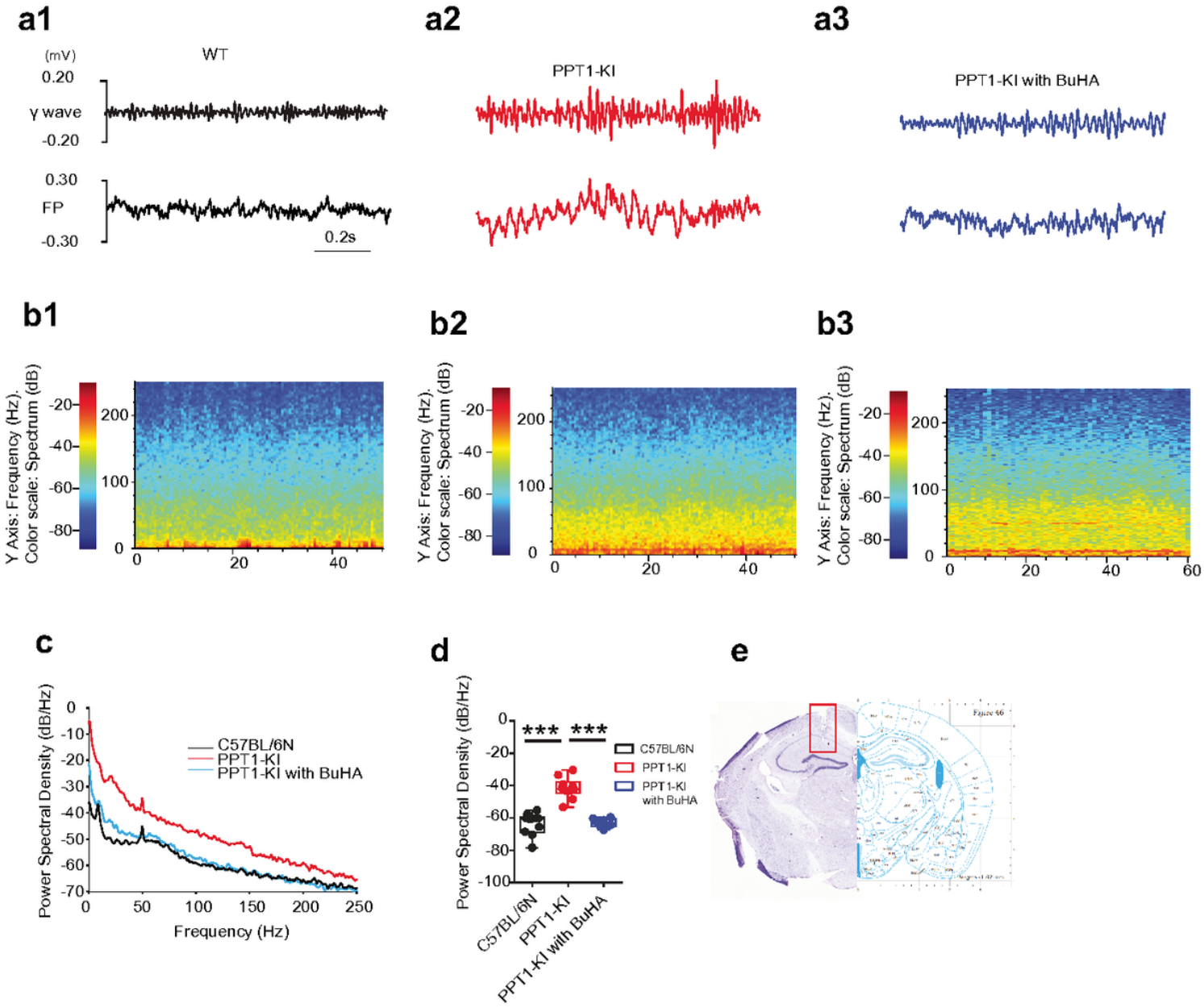

Figure 4

PPT1 deficiency enhances γ oscillation in young mice CA1 region.

(a1-a3) LFP signals recorded at CA1 region from wildtype **(a1)** PPT1-KI **(a2)** and PPT1-KI treated with BuHA **(a3)** mice (1 month of age). The upper traces displayed γ oscillation (30-80 Hz) band-pass filtered from LFP signals.

(b1-b3) Spectrograms of LFP signals recorded from wildtype **(b1)** PPT1-KI **(b2)** and PPT1-KI treated with BuHA **(b3)** groups (1 month of age).

(c) Power spectral density of LFP recorded from C57BL/6N (black curve), PPT1-KI (red curve) and PPT1-KI with BuHA (blued curve) mice (1 month of age).

(d) Statistical result of γ power spectral density (C57BL/6N: n=10 mice; PPT1-KI: n=10 mice; PPT1-KI treated with BuHA: n=8 mice, ***P< 0.001). Data are represented as mean ± SEM.

(e) Nissl stain indicating the electrode track.

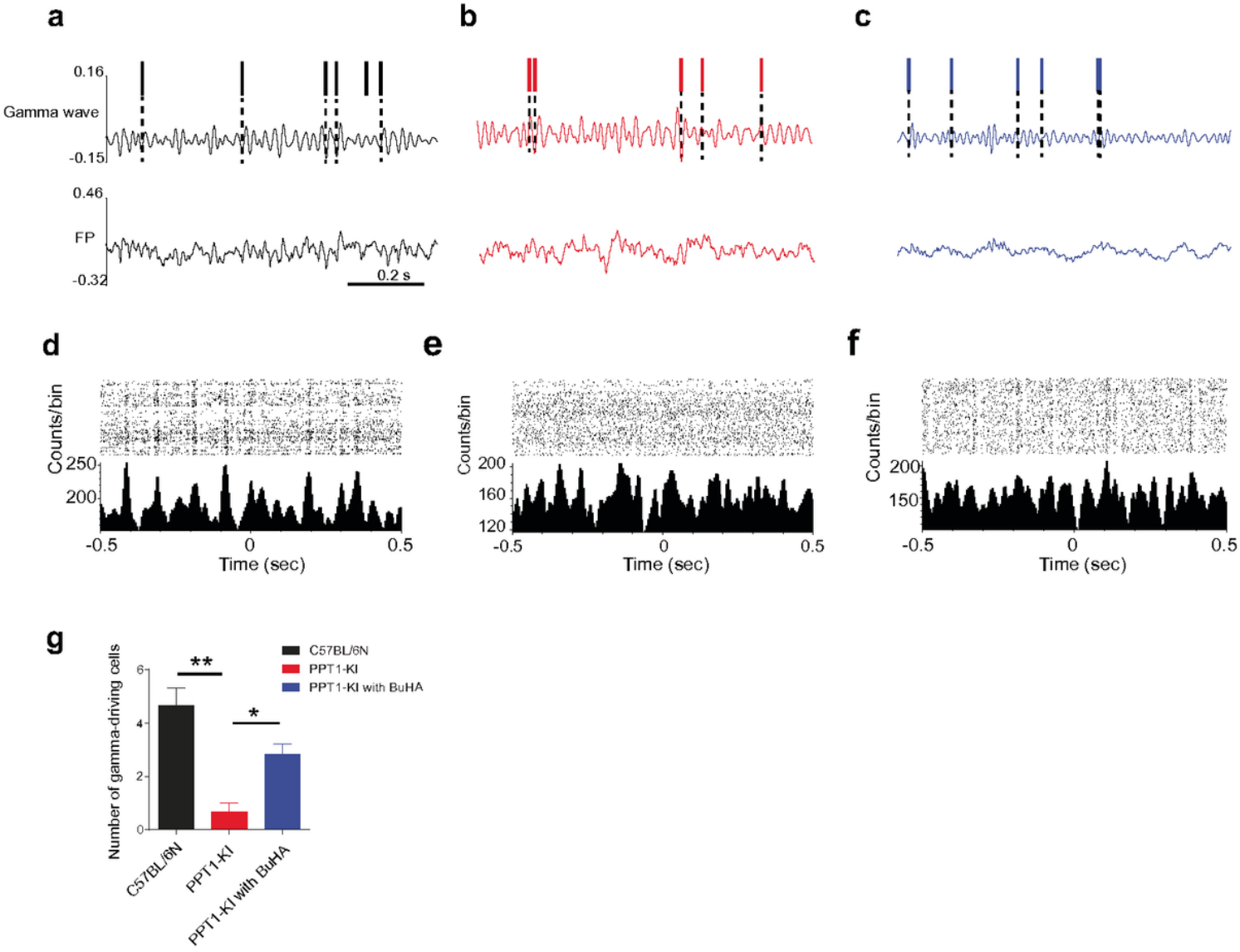

Figure 5

PPT1 deficiency attenuates γ phase-locking.

(a-c) Sampled traces showing the phase locking relation of spike unit recorded at CA1 from C57BL/6N (**a**, black trace), PPT1-KI (**b**, red trace) and PPT1-KI treated with BuHA (**c**, blue trace), and γ waves band-pass filtered from FP signals. The tips displaying timestamps of spike units. Scale bar: 0.2 s.

(d-f) Perievent raster of spike units and γ waves.

(g) Number of gamma phase-coupling neurons (C57BL/6N: n=6 neurons from 8 mice; PPT1-KI: n=6 neurons from 20 mice; PPT1-KI treated with BuHA: n=6 neurons from 18 mice; *P< 0.05, **P< 0.01). Data

are represented as mean ± SEM.

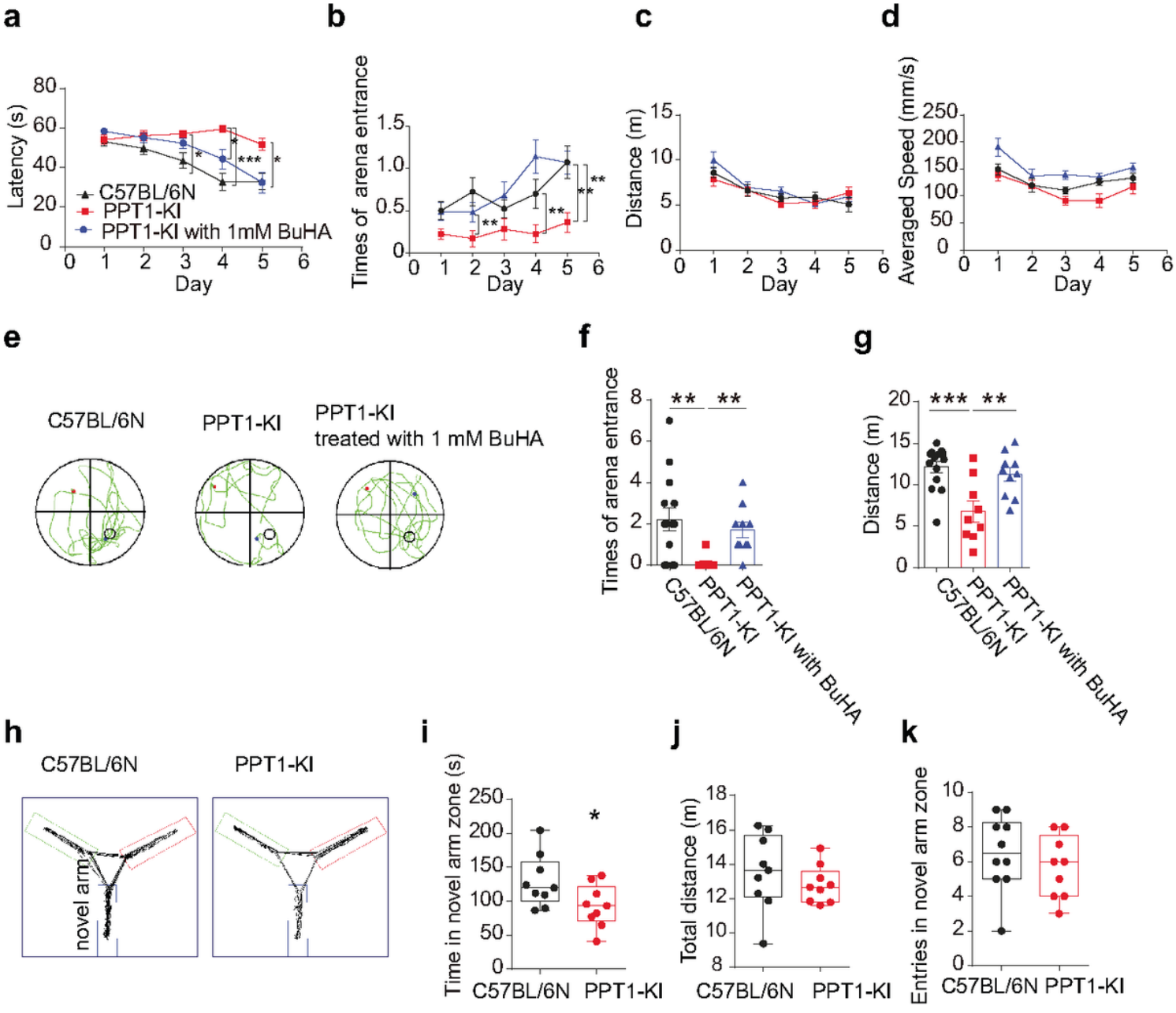

Figure 6

PPT1 deficiency mice exhibit spatial learning and memory deficits.

(a, b) Average latency to reach the hidden platform **(a)** and times entering the platform area **(b)** over five days of acquisition. One-way ANOVA test, **P*< 0.05, ***P*< 0.01, ****P*< 0.001.

(c, d) Total distance **(c)** and averaged speed **(d)** over five days of acquisition.

(e) The representative paths of wildtype (wildtype; left track), PPT1-KI (middle track) and the PPT1-KI treated with 1 mM BuHA (right track) recorded at spatial probe test day.

(f, g) Times entering the platform area **(f)** and total distance **(g)** in test trial (day 6). One-way ANOVA test, *P< 0.05, **P< 0.01, ***P< 0.001.

(h) Path taken on Y maze test by wildtype (left track) and PPT1-KI (left track) mice.

(i-k) Time spent in novel arm zone **(i)**, total distance **(j)**, and times of novel arm entries in test trial **(k)**. n=9 for each group; t- test, *P< 0.05.

Data are represented as mean ± SEM.

Supplementary Files

This is a list of supplementary files associated with this preprint. Click to download.

- FigS1pointmutantion.eps
- FigS2GABAexpressionat7M.eps
- FigS3iGluRsABE.eps
- FigS4EPSCrecording.eps